Flow Heterogeneity and Factors Contributing to the Variability in Retinal Capillary Blood Flow

Srividya Neriyanuri,[1] Phillip Bedggood,[1] R. C. Andrew Symons,[1–4] and Andrew B. Metha[1]

[1]Department of Optometry and Vision Sciences, The University of Melbourne, Parkville, Victoria, Australia
[2]Department of Surgery, The University of Melbourne, Parkville, Victoria, Australia
[3]Centre for Eye Research Australia, East Melbourne, Victoria, Australia
[4]Department of Surgery, Alfred Hospital, Monash University, Melbourne, Victoria, Australia

Correspondence: Srividya Neriyanuri, Department of Optometry and Vision Sciences, The University of Melbourne, 200 Berkeley Street, Parkville, VIC 3010, Australia; drsrividyaneriyanuri@hotmail.com.

Received: December 15, 2022
Accepted: June 17, 2023
Published: July 14, 2023

Citation: Neriyanuri S, Bedggood P, Symons RCA, Metha AB. Flow heterogeneity and factors contributing to the variability in retinal capillary blood flow. *Invest Ophthalmol Vis Sci.* 2023;64(10):15. https://doi.org/10.1167/iovs.64.10.15

Purpose. Capillary flow plays an important role in the nourishment and maintenance of healthy neural tissue and can be observed directly and non-invasively in the living human retina. Despite their importance, patterns of normal capillary flow are not well understood due to limitations in spatial and temporal resolution of imaging data.

Methods. Capillary flow characteristics were studied in the retina of three healthy young individuals using a high-resolution adaptive optics ophthalmoscope. Imaging with frame rates of 200 to 300 frames per second was sufficient to capture details of the single-file flow of red blood cells in capillaries over the course of about 3 seconds.

Results. Erythrocyte velocities were measured from 72 neighboring vessels of the parafoveal capillary network for each subject. We observed strong variability among vessels within a given subject, and even within a given imaged field, across a range of capillary flow parameters including maximum and minimum velocities, pulsatility, abruptness of the systolic peak, and phase of the cardiac cycle. The observed variability was not well explained by "local" factors such as the vessel diameter, tortuosity, length, linear cell density, or hematocrit of the vessel. Within a vessel, a moderate relation between the velocities and hematocrit was noted, suggesting a redistribution of plasma between cells with changes in flow.

Conclusions. These observations advance our fundamental understanding of normal capillary physiology and raise questions regarding the potential role of network-level effects in explaining the observed flow heterogeneity.

Keywords: blood flow, retinal capillary, erythrocyte velocity, adaptive optics imaging, human, flow heterogeneity

The retina is exceptional for being the most metabolically active tissue in the body. Supporting the various cellular processes that enable visual function is a complex system of capillary networks with regional and corresponding functional specialization.[1] The density of vascular supply in a normal human retina is not homogeneous but is continuously variable both tangentially across its surface and radially in depth.[2] Supply difference requirements can be met by simple variations in anatomical densities; for example, the inner capillary supply at the macula is greater than is available to the peripheral retina, presumably to support the higher density of inner retinal cells nearer the fovea by way of increased areal density.[3] Although such regional differences in capillary densities clearly exist, it is not known whether the distribution of actual blood flow follow these differences or not. Heterogeneity of red blood cell transit speed through nearby capillary segments has been observed[4–7] and may imply a level of variability in capillary resistance, even within a single layer. Similar local mechanisms may give rise to observed heterogeneity in the flow of leukocytes, as well.[8,9]

This article provides detailed observations that might lead to insights into the differences in patterns of capillary flow and the local variables influencing the flow across the foveal vascular network. This understanding could help unveil interesting pathophysiological mechanisms behind selective regional (both laterally and in depth) disruptions seen in vasculopathies such as diabetic retinopathy[10–15] and add to our understanding of capillary blood flow generally.

In general, large retinal vessels are marked as healthy or diseased based on examining physical variables such as size, shape, color, and reflex of the vessel using standard ophthalmoscopic or color fundus photographic imaging. With the advent of adaptive optics (AO) imaging, structural variables at a much finer scale, such as vessel caliber, wall-to-lumen ratio, and tortuosity, have become discernable in small vessels such as capillaries and have been flagged as promising indicators for disease at ever earlier stages of the vasculopathy process.[16–18] However, physiological variables such as the resting flow state and stimulus-evoked flow changes might provide greater insights into normal functioning of retinal vessels, particularly the capillaries.[19]

The flow measures have potential to be labeled as "biomarkers" of preclinical disease, especially if they can be shown to be significant in initiating structural damage that becomes visible only in a later clinical stage. These include flow measures such as cell speeds through a vascular segment and the variability (i.e., heterogeneity) of cell speeds in a small vascular bed region. Pulsatility is one such flow-derived functional measure that has been reported in both mouse and human retinal capillaries, where a clear time-dependent variability in flow is seen during systolic and diastolic phases of the cardiac pulse.[4,5,20–22]

AO imaging was used to identify the erythrocyte aggregates in parafoveal capillaries.[23] It was shown that the presence of erythrocyte aggregates (seen as dark tails and suggesting increased hematocrit) significantly increased the average velocities compared to vessels without the aggregates. The network dynamics further influenced the velocities at the bifurcations, where the daughter vessels with dark tails had lower velocities compared to the parent vessels with tails.[24] In addition to the role of erythrocyte aggregates, leukocytes also play a role in producing variability, as the lumen is blocked by the white blood cells, so erythrocytes bank up behind it (with plasma assumedly flowing past). Studies have shown specific leukocyte paths with variable flow speed and hematocrit resulting from the intermittent passage of leukocytes.[9]

As described above, retinal vascular diseases such as diabetes affect different regions of retina to varying degrees. Documenting the variations in flow patterns in smaller blood vessels may help in determining why some retinal locations (or some vessels in particular) are more or less prone to damage. Apart from the disease significance of lost capillary function in conditions such as stroke and dementia, studying the variability in normal capillary flow improves our understanding of the basic mechanisms of blood flow. Hence, the objectives of this study were as follows.

First, we wanted to observe and characterize spatial heterogeneity in capillary flow, which can also be termed "inter-vessel variability"; this is the degree to which adjacent foveal capillary segments support similar or dissimilar flow patterns. Structural variables within and/or at the vessel site might influence the characteristics of cellular flow (e.g., average velocity, maximum and minimum velocities) through any given vessel segment. Structural measures of potential relevance are the diameter, length, and tortuosity of vessels. Resistance to flow is classically (in larger vessels) proportional to the fourth power of vessel diameter; in the capillaries, the resistance to flow may be even greater than expected by this relationship.[25] Resistance is further proportional to the length of the vessel through which blood must traverse. Resistance is not expected to depend on vessel tortuosity at the microvascular scale due to the dominance of viscous rather than inertial forces in such vessels.[26] In addition to structural factors pertaining to individual blood vessels, the composition of the blood column may alter flow dynamics. Prior adaptive optics work has shown that the presence of erythrocyte aggregates in slightly larger vessels than those considered here (diameter >7–8 µm) tends to show faster flow.[23,24] Recent work from our laboratory has also shown that the separation between successive red blood cells is strongly linked to the shape of individual cells, suggesting that the forces experienced by a cell may depend on the composition of the blood column.[25]

Our second objective in the present work was to explore the extent to which the observed flow patterns may be affected by local (within the vessel) factors, including the vessel diameter, length, tortuosity, and composition of the blood column expressed by the linear cell density or by the hematocrit. The goal of comparing these variables is to try to form explanatory models of flow in the retinal capillary bed. The basic "rules" describing retinal capillary flow patterns are not well understood, and sophisticated computer simulations are required to predict flow.[27–29] Even such work does not typically consider pulsatile input at all, which is now known to be a feature of flow in all retinal capillaries analyzed to date. In the absence of a simple model, the first step in the chain of inquiry ought to be consideration of the basic statistical patterns (e.g., covariance among available outcome measures), as well as normative data.

Methods

The study was approved by the Human Research Ethics Committee of The University of Melbourne (ethics approval number 1137234) and adhered to the tenets of the Declaration of Helsinki. Written informed consent was obtained from all study participants, and all study procedures were clearly explained prior to the study protocol being initiated.

Three healthy individuals (one male and two females; age range, 22–23 years) who were free from any known ocular or systemic illnesses participated in this study. Participants with clear media and a refractive error of less than 4 diopters (D) spherical and 2 D astigmatic error were considered suitable for small vessel imaging. The left eye of each participant was chosen for vascular imaging using optical coherence tomography angiography (OCTA) (SPECTRALIS; Heidelberg Engineering, Heidelberg, Germany) and AO (custom "flood" illuminated system described below). Pupils were pharmacologically dilated using 0.5% tropicamide (Alcon, Geneva, Switzerland) at least 20 minutes prior to the AO imaging.

The structural information from OCTA was used as a guide to image the vessels around the foveal avascular zone (FAZ) using AO, which formed the main investigative tool for the study. The principles and implementation of the AO imaging system have been described in detail in previously published articles[7,30–32] and are described briefly here.

AO Imaging Procedure

The image capturing part of the AO setup consisted of a 2560 × 2160-pixel Andor NEO sCMOS camera (Andor Technology PLC, Belfast, UK), which enabled the fast image acquisition rates required for tracking blood flow (in this work, 200–300 fps). All pixels were exposed simultaneously using the Global Shutter mode of the camera, resulting in images that were free of intra-frame distortion due to eye movements. The ocular wavefront aberrations were measured using a Hartmann–Shack wavefront sensor (Adaptive Optics Associates, Devens, MA, USA). Measured wavefront slopes were corrected by a 97-channel deformable mirror (ALPAO, Montbonnot-Saint-Martin, France) in real time using a closed-loop control operating at 30 fps by custom MATLAB software (version R2017a; MathWorks, Natick, MA, USA). The best focus of the blood vessels was achieved by adjusting the defocus component of the adaptive optics correction in 0.05-D steps. The criterion was set such that the appearance of cellular flow within the maximum number of capillaries in the field was subjectively maximized (as opposed to, for example, vessel walls or larger sized vessels). The depth of focus of our system is such

that this can be done reliably to the nearest 0.05 D (typical) or 0.10 D (in the case of poorer image quality). Even finer adjustments are discernible when using a (stationary) model eye of similar numerical aperture to a human eye.

Imaging Procedure. Small patches of the foveal microvascular network that were 1.25° (approximately 360 µm) in diameter were imaged using a 750-nm light (supercontinuum laser passed through a tunable SuperChrome transmission filter, SC480-8; Fianium, Southampton, UK) in a darkened laboratory. This light resulted in a power of 0.36 mW at the cornea, which adhered to the American National Standards Institute guidelines of maximum permissible exposure standards for continuous illumination over 3.4 seconds and was at least 10 times safer than the standard.[33] The fixation target used was a diffusely back-illuminated fixation grid printed in black on white paper. The imaging area was centered 1° to 2.5° from fixation, around the FAZ, and the participant was asked to stare at the appropriate location on the fixation target to bring each region of interest into the field of view. The vertical extent of the imaging field was set to either 512 pixels (covering approximately 0.89° or 256 µm on the human retina) to achieve a frame rate of 200 fps or to 328 pixels (164 µm) to achieve a frame rate of 300 fps under the Global Shutter setting. The horizontal extent of the imaging field was not limited by frame-rate considerations and was set by a field stop to span 1.25° diameter (360 µm). The frame rate was adjusted to attempt maximizing the amount of useful information captured from a given capillary network. For example, in an area of slower flow, a slower frame rate could be chosen, permitting a taller field size and hence a larger number of vessels captured. If flow was too fast, however, the higher frame rate with fewer rows in the image would be required to capture more of the flow. This judgment was made on an ad hoc basis in each imaged field. The imaging was done using different frame rates of 200 or 300 frames per second (fps) for a maximum of 3.4 seconds to create a video sequence for the calculation of flow velocity, described below. Videos of greater duration could not be recorded due to memory bandwidth limitations in transferring data from the camera to our computer. However, much longer recording periods would not typically be desirable due to variations in tear film, associated blinking, and difficulty in maintaining steady fixation over longer periods.

It should be noted that our acquisition was not synchronized to the activity of the heart (for example, triggered based on the electrocardiogram waveform). Although cardiac activity is an extremely important source of variability, a variable lag among subjects is expected, resulting from differences in the electrical activity of the heart, its subsequent muscular contraction, and propagation of the pulse wave along the vascular tree before finally reaching the retinal capillaries. To ensure we fully captured variability due to cardiac contractility, we recorded over ~3 seconds (around three full cardiac cycles). For the comparison of the phase of velocity waveforms across vessels, we therefore restricted our analysis to just those vessels imaged at the same time within our field of view.

Spatial Heterogeneity

The variability in velocities between vessels across the network is referred to here as spatial heterogeneity, which was studied by examining the capillary vessel flow patterns from neighboring retinal fields surrounding the FAZ.

Extracting Cell Velocities. Figure 1 shows how an individual vessel segment was chosen and used for velocity analysis in one of the subjects. First, a suitable region for imaging was identified from the OCTA map (Fig. 1A). A motion contrast image was generated from AO video data in all chosen regions,[34] and all such images were combined to generate a high-resolution montage (Fig. 1B). From the motion contrast montage, the complete vascular network skeleton was manually traced using Photoshop (Adobe, San Jose, CA, USA). As an initial step in data processing, raw video sequences were manually inspected to identify vessels with sufficiently high contrast, slow flow, and sparse hematocrit that cellular flow could be tracked unambiguously throughout the full cardiac cycle (an example selected vessel is shown in Figs. 1C and 1D). No vessels containing putative leukocyte flow were included for analysis. For vessels manually approved for analysis in this way, red cell velocity through time was computed within a rolling epoch 150 ms in duration from the AO video data using a kymograph approach.[35] The epoch (100–150 ms) chosen was somewhat arbitrary. A sufficient number of frames are required to produce an accurate velocity estimate; however, if too many frames are used, this will compromise the ability to track sudden changes in velocity. Epochs of 100 ms (300 fps) and 150 ms (200 fps) were chosen as a trade-off among these factors and are comparable to epochs chosen in previous studies.[5,20,21]

As shown in Figure 2, velocities (given by a slope) were estimated using three standard approaches: spatiotemporal (ST) plot and two-dimensional (2D) spatial and 2D temporal correlograms. The best estimate was taken from the approach that provided the highest signal-to-noise ratio.[35] As reported in our previous study,[35] the spatial and temporal correlograms were deemed more reliable than the ST plot in the majority of epochs analyzed. In this study, across several thousand epochs, the temporal correlogram was selected in 70% of epochs, the spatial correlogram in 26%, and the ST plot in 4% of epochs. If the slope given by an approach did not appear to visually match with the flow information presented in a window, the best of the three approaches was picked subjectively (i.e., by the human supervisor), and the velocity information was overwritten for that window. In rare cases where all three approaches failed to pick up a slope that matched the direction of the flow information determined subjectively, the velocity for that window was flagged as "NaN" (not a number) and excluded from the analysis (Fig. 2C). Epochs were excluded where the kymograph appeared to display flow in the reverse direction, which often indicates aliasing. Upon detailed analysis, of a total of 2956 epochs analyzed across 72 vessels, 10 individual epochs were excluded. About 10 to 15 neighboring vascular segments within each field were considered suitable for velocity analysis. It is worth noting that, for this study, we did not use a recent, more robust automated method published by our group[21] because it was not available at the time of commencement of this study.

Parameters Derived From Velocity–Time Plots. The velocity–time plots (i.e., average epochal velocities plotted as a function of time for each vessel, also described as velocity plots) were derived from included data for all the vessels. The following flow measures were directly extracted from the velocity–time plot (blue data points in Fig. 3) for each vessel segment: The average velocity (V_{ave}), defined as the mean over the full time period observed (minimum 3 seconds), and the maximum or peak velocity (V_{max_raw}), as

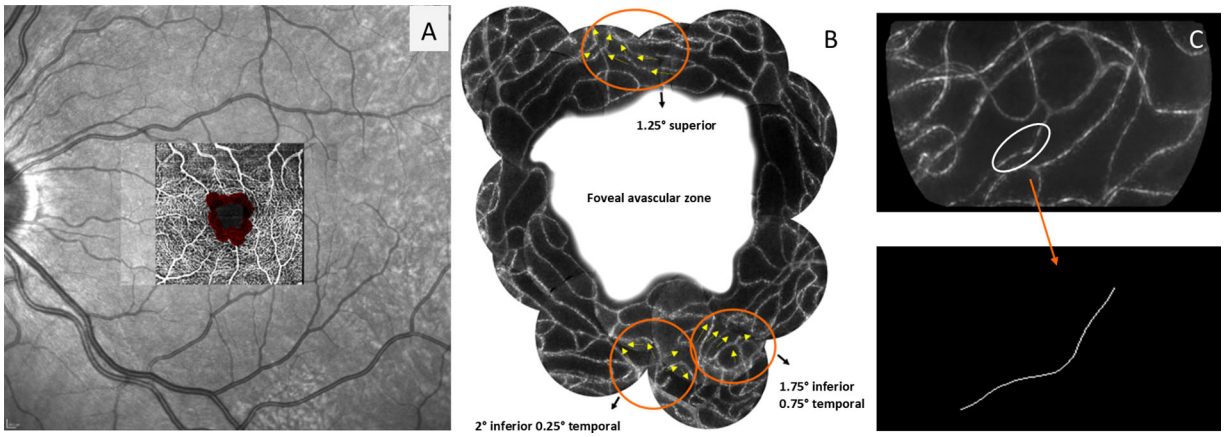

Figure 1. Identifying a vessel segment of interest. (**A**) Retinal fundus scanning laser ophthalmoscope (SLO) and SPECTRALIS OCTA. The area in *red* indicates the region imaged using AO. (**B**) AO montage highlighting regions of interest (*encircled*; *yellow arrows* indicate flow direction). (**C**, **D**) Division image highlighting a vessel segment of interest (**C**) whose skeleton (**D**) was used for constructing a velocity plot.

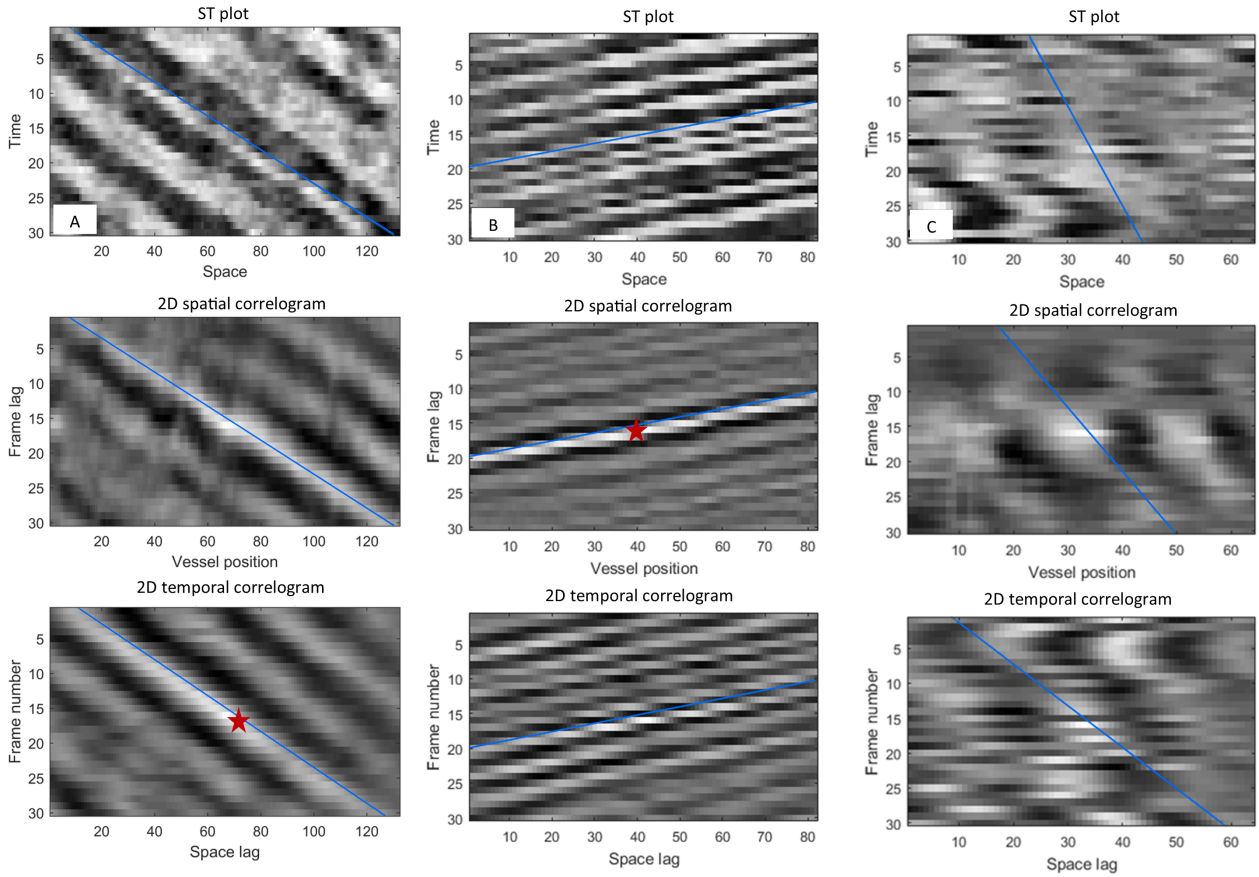

Figure 2. Examples showing Kymograph analysis. (**A**, **B**) Good examples of kymographs from subjects 1 and 2, respectively, showing that all three approaches estimated reliable velocities (indicated by a slope in *blue*). The example shows an approach picked as "best" (indicated by *red star*) by the algorithm based on a high signal-to-noise ratio. (**C**) An example in which all three approaches failed to pick up a best slope and hence the velocity for this window was taken to be not a number (NaN).

well as minimum or trough velocity (V_{min_raw}), were noted across all epochs and quantified for each vessel segment. The deviation or dispersion of cell speeds from the mean in the video of a given vessel was given by velocity standard deviation (V_{stdev}), and a normalized measure of velocity variability was given by the coefficient of variation (COV), calculated as V_{stdev}/V_{ave}.

To capture key information regarding flow dynamics within each vessel, we fitted a triangular-wave parametric curve to the data for velocity over time (blue data points

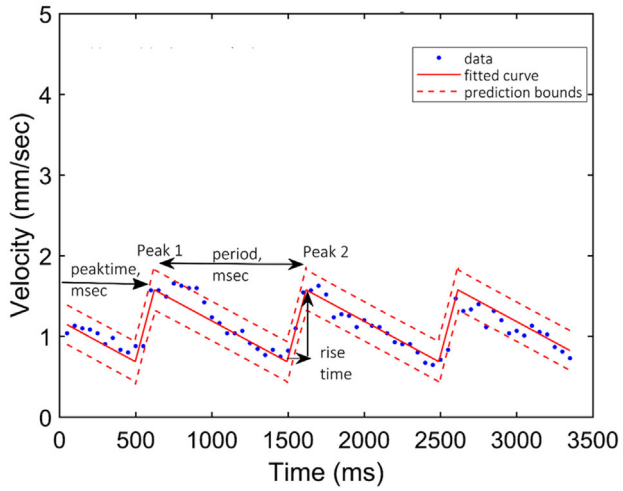

Figure 3. Triangle-wave curve fit for velocity plot. Raw velocity estimates plotted against time are shown in *blue points*. Each data point shows cellular flow velocity through a given capillary segment within a single epoch (100 ms). A fitted curve is shown as a *solid red line* for raw velocity information plotted over 3 seconds of data (points in *blue*) for a single vessel. *Dashed red lines* indicates 95% bounds for the fitted data.

in Fig. 3). This was performed using standard MATLAB curve fitting routines (we used the Fit function of the MATLAB R2017a Curve Fitting toolbox), and 95% confidence intervals (CIs) for the data were also returned, as shown in Figure 3. The fitted velocity traces were generally well modeled by this simple curve fit approach, with average R^2 of 0.78 ± 0.17 (mean ± SD). The velocity data for each vessel were fitted for five essential key parameters: (1) maximum velocity ($V_{max\_curvefit}$); (2) minimum velocity ($V_{min\_curvefit}$); (3) peak time (time taken for the onset of first peak); (4) period (time between consecutive peaks); and (5) abruptness (defined as a proportion of the period with rising velocity and calculated as "rise time/period"). Pulsatility was defined by calculating $(V_{max} - V_{min})/(V_{max} + V_{min})$.

Measuring Local Vessel Structure Variables

In order to study and predict the velocity variations within a network, we measured local vessel structural variables and other local flow variables such as linear cell density (LCD) and hematocrit.

Vessel Diameters. Using registered "division" images to represent our best information regarding the internal lumen diameters of vessel segments, vessel diameters were measured in MATLAB by applying the Otsu automatic image thresholding method for detecting edges.[36] To threshold each vessel, pixels were removed from the image that were closer to another vessel (creating a region of interest containing only the vessel and pixels in the background).

A maximum likelihood curve was fitted to the binary "above threshold or below threshold" image data, with the edge of the vessels chosen as the 50% probability point. The thresholded image data were bootstrapped by randomly selecting, with replacement, the pixels to be included in the likelihood curve. Confidence intervals were thus generated by sorting the bootstrapped diameter measures, with narrow intervals indicating robust measurement of internal vessel diameter.

Vessel lengths were calculated in pixel units from the one-pixel skeletonized segments between bifurcations. The vessel lengths reported here represent the full length of the vessel between two bifurcations. Vessel tortuosity was defined as the ratio between the length of the vessel to the shortest distance between the start and end of the vessel segment. Vessel length was calculated using the following conversion: 1 pixel = 0.5 µm, based on the paraxial magnification expected for our system in imaging an emmetropic eye with a focal length of $f = 17$ mm in air; this is an approximate figure only, with refraction ranging up to 4 D in our subjects.

Measuring Local Vessel Flow Variables

The local vessel flow variables that were studied are LCD (number of cells per millimeter length of vessel) and hematocrit (fraction of blood column occupied by erythrocytes). The LCD for a vessel segment was defined as the number of cells per unit length of vessel segment. The hematocrit content of a vessel was measured as a ratio of the length of cells occupying a vessel to the length of vessel analyzed. Both measures require that the cells occupying a vessel segment are delineated. This was achieved by motion correct of the XT plot, which has been described elsewhere.[37] In brief, the approach is to shift each row of the kymograph according to the flow velocity, producing a "stationary" XT plot in which vertical bright and dark vertical bands correspond to cells and plasma (Fig. 4B).

The fundamental assumption underlying the shifting of data in horizontal rows is that the blood column is a fluid and should therefore be incompressible. Within a rigid tube we would expect the entire blood column to travel at the same speed even during the systolic transition. However, it may be noted that, if the capillary tube is not entirely rigid, then differences in speed along the blood column should manifest—for example, as acceleration lag due to the finite propagation speed of the pulse pressure wave.

This is a subtle signal that can be revealed in many capillary vessels with our approach.[38] Overall, however, the high speed of the pulse wave compared with the much slower speed of blood flow is such that the analysis method described in Figure 4 (based on incompressibility of fluid) is a good approximation to compensate for the motion of the blood constituents; that is, the entire blood column can be presumed to travel at the same speed. It should be noted that the point of compensating for cellular motion (i.e., rendering them as straight vertical bars) is that it allows data from each cell to easily be averaged over time. This dramatically improves the signal-to-noise ratio for image segmentation, greatly aiding computation of the hematocrit compared with (for example) simply applying standard automated thresholding approaches to the kymograph. Because either cells or plasma can appear with positive contrast depending on the plane of focus,[35] video data were manually inspected to confirm the identity of cells; in cases where this judgment was difficult, the vessel was excluded from analysis.

To delineate cells, a brute force approach was adopted in which binary image masks consisting of a series of bars were fit to the motion-corrected kymograph. The free parameters were the location, width, and number of bars. The mask giving the greatest statistical difference (P value of t-test) between the intensity of pixels inside and outside the mask

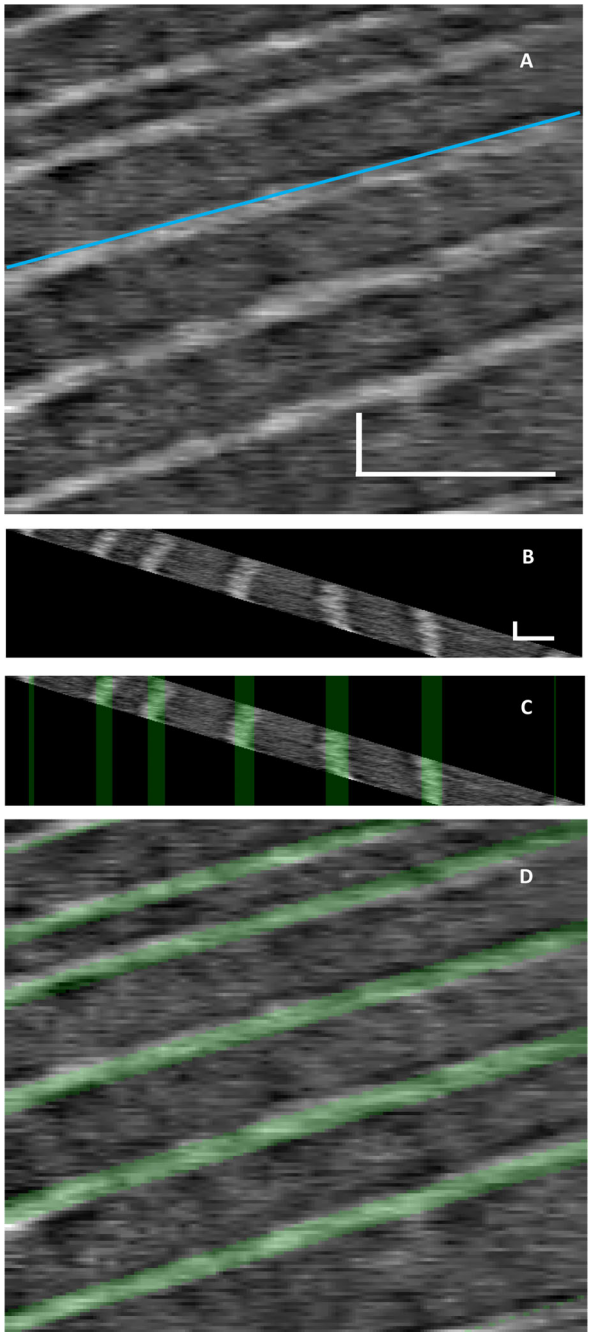

Figure 4. Counting red blood cells. (**A**) Kymograph shows intensity along a vessel centerline as a function of time. Slope given by the *blue line* indicates the flow velocity (~0.11 mm/s). (**B**) Motion-corrected kymograph obtained by cumulatively sliding each row of **A** according to the flow velocity. (**C**) As for **B** but with a binary mask overlaid to indicate the position of found cells (see text). (**D**) Binary mask from **C** projected onto the original kymograph from **A**. *Scale bar*: 20 µm horizontal and 100 ms vertical.

was taken as the one most faithfully delineating cells from plasma.

Statistical Analysis of the Data

Further statistical analysis of the data was performed using SPSS Statistics 21.0 for Windows (IBM Corp., Chicago, IL, USA). The SPSS Statistics software was used to scrutinize the distribution of the parameters and discern correlations among them. Correlations among parameters were examined using the two-tailed Pearson's test at a significance level of 0.05. Correlation coefficients between 0.00 and 0.30 were considered to indicate negligible correlation; 0.30 to 0.50, low correlation; 0.50 to 0.70, moderate correlation; and 0.70 to 0.90, high correlation.[39]

Results

This section presents data concerning the flow of red blood cells tracked through 72 different retinal capillary segments (13 different fields of interest) from three subjects. The numbers of vessels analyzed for each subject were 20, 34, and 18, respectively. As described in the Table, the variables are categorized as either flow parameters or as local structural or flow variables.

General Flow Characteristics

Each vessel segment from three subjects (total of 72 vessels) was quantified for flow parameters (Table). For each AO video, a peak-time offset for each vessel was calculated by subtracting the individual peak times from the average peak time (of all the vessels within a given field). The peak-time offset serves as a dispersion measure for the relative phase of the cardiac cycle through vessels in the field. The peak-time offsets in a field ranged from 4.6 ms to −230.3 ms. Approximate heart rates (calculated as 1/period × 60 seconds) ranged between a minimum of 48 and a maximum of 94 beats per minute.

Variability Within Individual Subjects

When studied within single subjects, variations in the spread of flow parameters were observed across different retinal fields. Data from two subjects are presented here (Fig. 5). As an example, the average velocities ranged between 0.5 and 2.0 mm/s, the maximum velocities varied between 0.8 and 3.0 mm/s in a subject, and the peak-time offsets ranged from 13 ms to −128 ms. Within a subject, maximum velocity (noted across different retinal fields) was manifestly correlated with average velocity, as expected (Fig. 5A). However, no such significant relations were noted for abruptness, pulsatility and the peak-time offsets (Figs. 5B–5D).

Spatial Heterogeneity. Spatial heterogeneity in the characteristics of cellular flow through nearby capillaries (as described earlier) was observed by analyzing a minimum of three and a maximum of 10 adjacent vessel segments from each field that had been imaged contemporaneously. This was assessed in different retinal fields across our three study subjects.

An example for spatial heterogeneity within a retinal field 1.25° superior (to the FAZ) is shown in Figure 6, where the variability in flow parameters among neighboring vessels is clearly shown. A quick rise time (low abruptness) is seen in vessel segment "e," whereas in contrast segment "i" shows an abruptness as high as 0.38 (indicating a slow rise time). Similarly, a great variability in peak-time offset can be seen within neighboring vessels (in a retinal field 1.75° inferior and 0.5° temporal); one vessel has an offset of −34 ms whereas another vessel within the same field has an offset

Investigative Ophthalmology & Visual Science

Table. Descriptive Statistics of the Flow Parameters and Local Structural Variables

	N	Mean ± SD	95% CI	Range
Flow Parameters				
V_{ave} (mm/s)	72	1.18 ± 0.46	1.07–1.28	0.26–2.30
V_{stdev} (mm/s)	72	0.33 ± 0.15	0.30–0.37	0.11–0.76
V_{max} (mm/s), raw	72	1.87 ± 0.73	1.70–2.04	0.61–3.73
V_{min} (mm/s), raw	72	0.65 ± 0.31	0.58–0.73	0.09–1.40
Coefficient of variation (V_{stdev}/V_{ave})	72	0.29 ± 0.65	0.27–0.30	0.20–0.50
V_{max} (mm/s), curve fit	72	1.70 ± 0.66	1.55–1.86	0.45–3.45
V_{min} (mm/s), curve fit	72	0.65 ± 0.28	0.59–0.72	0.08–1.35
Peak time (ms)	72	621 ± 253.90	562.34–681.91	103.97–1093.84
Period (ms)	72	908.51 ± 85.87	887.93–928.28	638.15–1236.46
Pulsatility contrast	72	0.45 ± 0.10	0.42–0.47	0.25–0.72
Abruptness	72	0.18 ± 0.13	0.15–0.21	0.00–0.74
Local Structural Variables				
Diameter (µm)	72	4.33 ± 0.90	4.11–4.54	3.00–7.75
Tortuosity	46	1.31 ± 0.40	1.19–1.43	1.06–2.73
Vessel length (µm)	46	230.36 ± 128.48	192.21–268.52	32.73–702.17
Local flow variables				
Linear cell density (cells/mm)	59	48.06 ± 14.84	44.19–51.93	23.66–93.67
Hematocrit (%)	59	0.41 ± 0.08	0.39–0.43	0.24–0.57

N indicates number of capillary vessels. Low abruptness value indicates a quick rise time and vice versa.

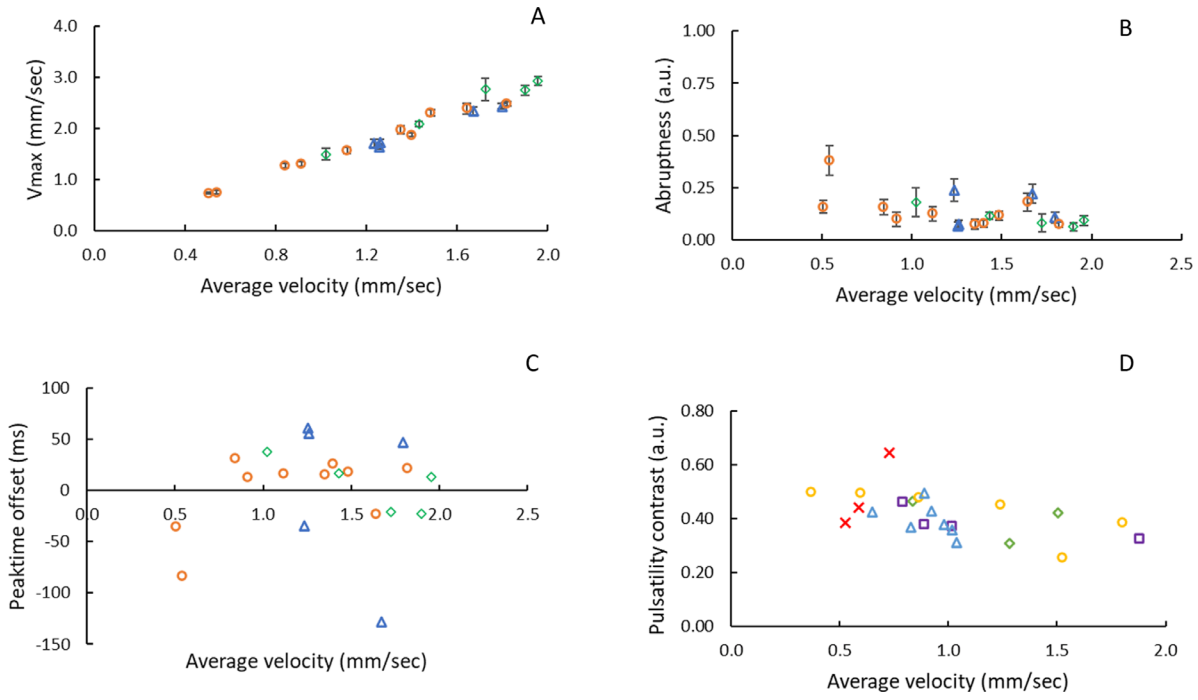

Figure 5. Scatterplots representing the spread of flow parameters as a function of average velocity. (**A–C**) Spread of V_{max} (**A**), spread of abruptness (**B**), and spread of peak time offset (**C**). Points in different colors and symbols represent data from retinal locations 1.75° inferior, 0.75° temporal (in *triangle*, *blue*), 1.25° superior (in *circle*, *orange*), 2.25° inferior, and 0.5° temporal (in *diamond*, *green*) from subject 1. (**D**) Spread of pulsatility in subject 2. a.u., Arbitrary unit. Colored (and shaped) points represent data from retinal locations 0.5° inferior, 1.5° temporal (in *diamond*, *green*), 1° superior (in *circle*, *yellow*), 1° nasal, and 0.5° inferior (in *square*, *purple*) and 1° temporal, 1° superior (in *cross*, *red*), 2° inferior, and 0.5° temporal (in *triangle*, *blue*) from subject 2. *Error bars* indicate 95% CIs on curve-fit parameters.

of −128 ms, which indicates a significant dispersion in peak times within a field.

We estimated the pulse wave velocity (PWV) of propagation by comparing the path difference and time difference in the peaks for neighboring vessels within a retinal field. For example, the PWV for the field presented in Figure 6 was calculated using feeder distance and the peak times for two sample vessels—namely, segment "g" and segment "a"

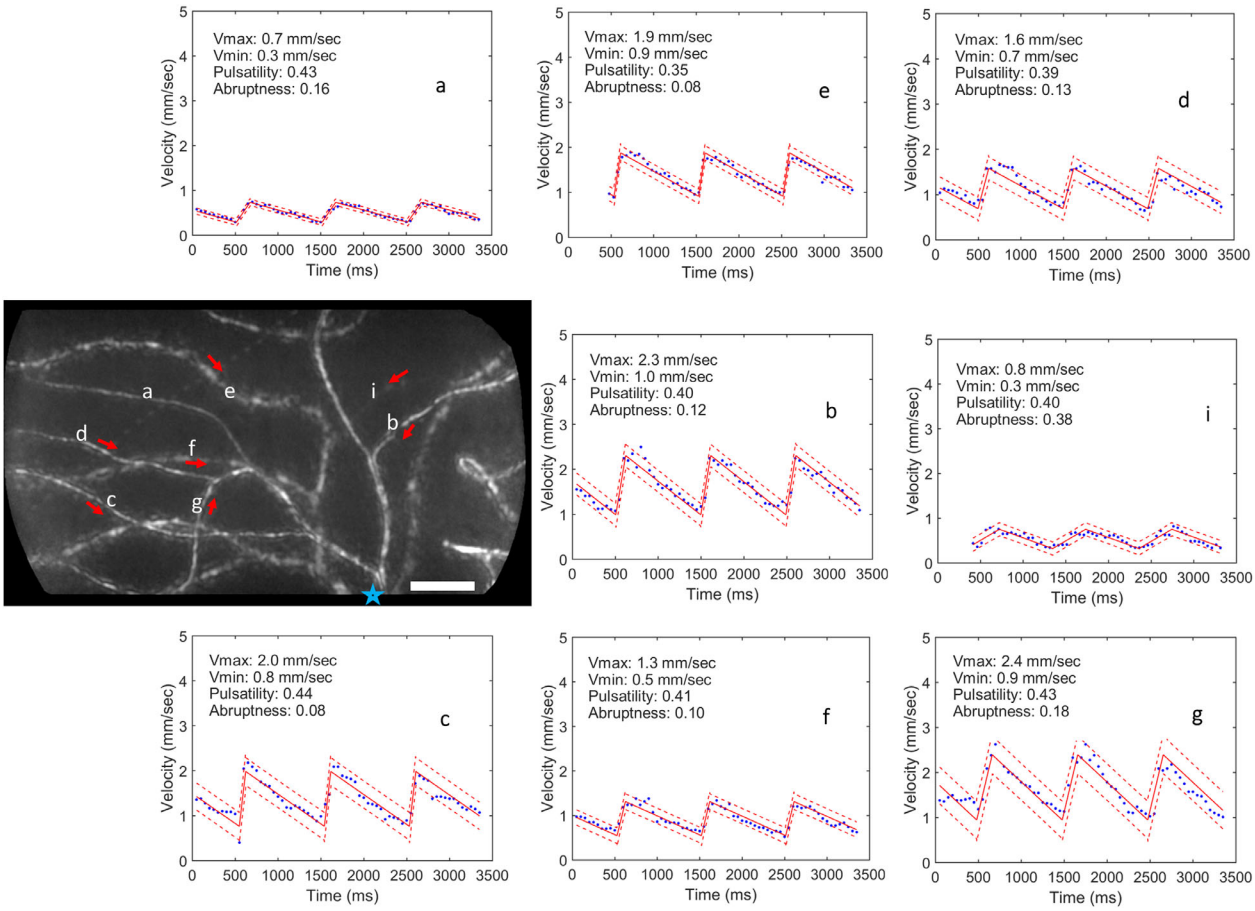

Figure 6. Spatial heterogeneity of velocity plots within an imaged field. Curve fitted velocity plots for neighboring vessels from a field 1.25° superior to the FAZ from subject 1 (unique vessels are indicated by an alphabetical label and their corresponding velocity plots are presented). *Arrows* indicate blood flow direction; the venous end is indicated by a *blue star*. *Scale bar*: 50 µm.

as follows:

$$\begin{aligned}\text{PWV} &= (\text{feeder distance 1} - \text{feeder distance 2})/\\ &\quad (\text{time to peak 1} - \text{time to peak 2})\\ \text{PWV} &= (517.68 - 385.97)/(674.17 - 661.83) = 11 \text{ mm/s}\end{aligned} \quad (1)$$

This is comparable to what has been reported by Bedggood and Metha.[38]

Within each retinal field across our three study subjects, adjacent vessel segments exhibited variable flow patterns. For example, the greatest variations in pulsatility ranged between 0.28 and 0.71 within a single field. Similarly, V_{max} ranged between 0.7 and 2.7, and V_{min} ranged between 0.3 and 1.2 mm/s within a single field.

Correlations of Flow Parameters and Local Vessel Variables

An exploratory data analysis was done to reveal any important associations in the dataset and the significant ones have been plotted here. Of a total of 15 independent correlations run between flow parameters and local vessel variables from a total of 72 vessel segments ($n = 3$ subjects), the following correlations were found to be statistically significant (Fig. 7).

Relation of Local Flow Variables to the Velocities

LCDs and hematocrits were analyzed and could be reliably computed for 59 of the 72 vessel segments (across all three subjects). These LCDs averaged to 48.06 ± 14.7 cells/mm (mean ± SD), and the hematocrits averaged to 0.41 ± 0.08. Figure 8 depicts the general distribution of these parameters with respect to a Gaussian fit. The LCD and hematocrit values were analyzed for their associations with the flow measures and possible structural variables. Among all of the possible associations between the variable sets of LCDs and hematocrits with the flow parameters (i.e., a total of 10 independent correlations were run), LCD was found to be positively correlated with vessel length ($r = 0.46$; $P = 0.004$; $n = 37$). A low negative correlation was noted between the LCD and V_{min_raw} ($r = -0.27$; $P = 0.034$; $n = 59$) (Fig. 9).

LCDs in general were positively correlated with the hematocrits, as noted across 59 vessel segments ($r = 0.51$; $P = 0.0001$). Unlike LCDs, however, no significant associations were found for average hematocrits across all vessel segments with any of the structural variables and flow

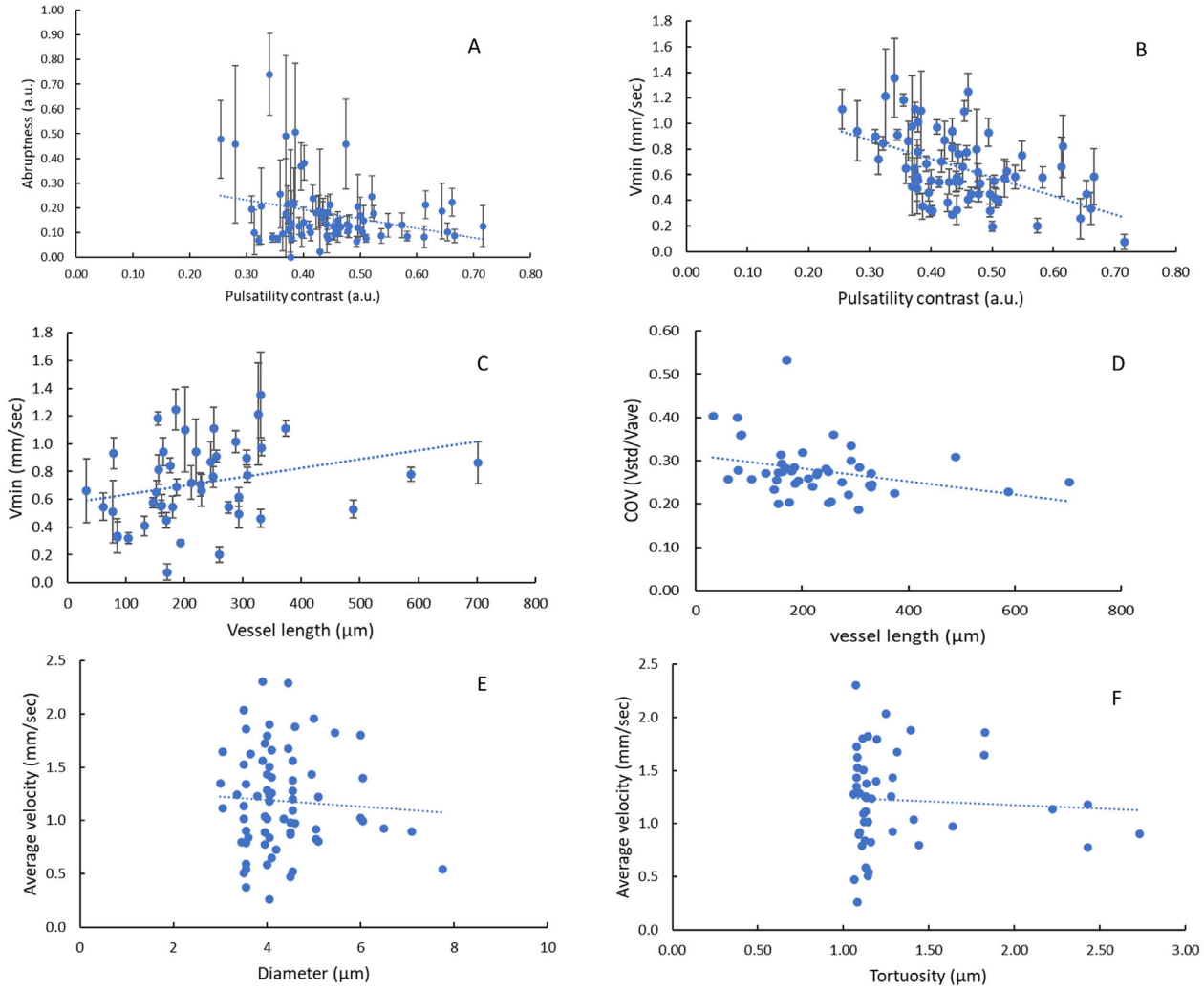

Figure 7. Scatterplot representing correlations between different flow and local vessel variables. (**A**, **B**) Correlations within the flow parameters: **A** ($r = -0.28$, $P = 0.016$) and **B** ($r = -0.49$, $P = 0.0001$). (**C**–**F**) Correlations between flow variables and local vessel structural variables: **C** ($r = 0.30$, $P = 0.045$), **D** ($r = -0.30$, $P = 0.038$), **E** ($r = -0.04$, $P = 0.701$), and **F** ($r = -0.10$, $P = 0.503$). *Error bars* represent 95% CIs on the curve-fit parameters of abruptness and V_{min}. The COV data do not show any error bars, as these are computed from raw measures (V_{ave} and V_{stdev}).

measures. In order to explore any relation of hematocrits with flow measures, instantaneous velocity and hematocrit (and LCD) variables were studied at the individual vessel level. Out of 59 vessels, nearly 50% of the vessels had a positive correlation between the hematocrit and the instantaneous velocity, and 37% of the vessels had a positive correlation between LCD and velocity.

To further illustrate some of the above correlations, some examples of significant relations from individual vessels are presented in Figures 9C and 9D. In a vessel segment from the retinal field 1.75° inferior and 0.75° temporal to FAZ in subject 1, an inverse relation was noted between instantaneous velocities and LCD ($r = -0.46$; $P < 0.001$). In another vessel segment from the same field, a moderate positive relation was noted between the instantaneous velocity and hematocrit ($r = 0.55$; $P < 0.001$).

Discussion

This study provides data and analysis that potentially offer insights into capillary flow characteristics in normal human retinas. One of the interesting findings from the present study is that the flow of red blood cells through one vessel segment can be quite different from the flow through its immediate neighbors (i.e., there is marked spatial flow heterogeneity). This was observed for a number of measures such as the average velocity, minimum velocity, maximum velocity, pulsatility, peak time, and abruptness within individuals, and within each retinal field.

Retinal Capillary Vessels Exhibit Pulsatility

One of the important observations from this study was that pulsatility in cellular flow was observed within all of the vessels in our subjects. This agrees with the results of studies in human subjects assessing 22 and 41 vessels.[4,5] We have confirmed this phenomenon in vessels ($n = 72$) exhibiting velocities ranging from a minimum of 0.1 mm/s to a maximum of 3.7 mm/s.

The overall erythrocyte pulsatility averaged 0.45 (range, 0.25–0.72), which is lower compared to two other studies,

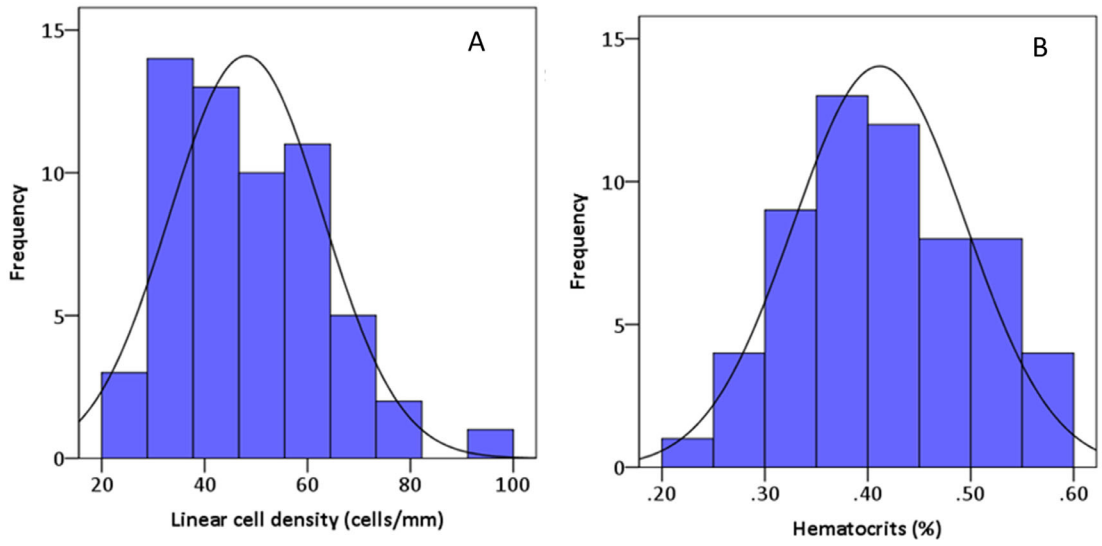

Figure 8. Histogram representations of LCD and hematocrit data. (**A**) Distribution of LCD showing a left skew relative to the normal Gaussian fit indicated as a *black bell-shaped curve*. (**B**) Normal distribution of hematocrit.

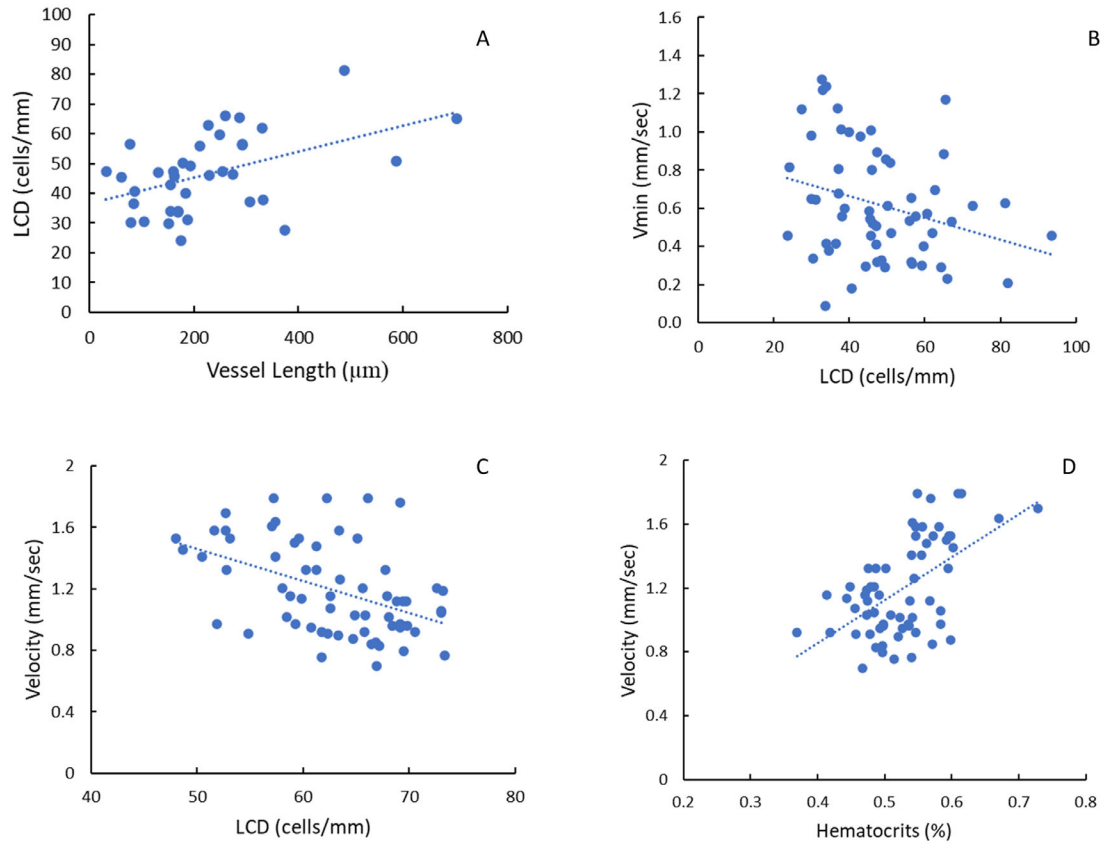

Figure 9. (**A**, **B**) Scatterplots representing the variability in LCD with vessel length (**A**) and V_{min_raw} (**B**). (**C**, **D**) Scatterplot representing relations between instantaneous velocity estimates and vessel flow variables within a single vessel segment. Data presented were taken from multiple short windows (of 100-ms width) within a single vessel.

which reported average pulsatility values of 0.79 (0.48–1.28)[4] and 0.91 (0.63–1.57),[5] similar to the leukocyte pulsatility range of 0.54–0.61 reported by Tam et al.[9] and pulsatility of 0.45 (0.31–0.65) reported by Martin and Roorda.[8] These studies measured pulsatility using $(V_{max} - V_{min})/V_{mean}$. In the current study, we calculated pulsatility using the formula $(V_{max} - V_{min})/(V_{max} + V_{min})$. This difference in the way pulsatility was measured would have resulted

in slightly lower values in our study as compared to other studies.

Capillary flow pulsatility is supported by the rhythmic action of the heart, where the alternating systolic and diastolic pressures of the cardiac cycle drives temporal variations in the velocities measured within the retinal capillaries.[4,5,19,21,22] The shape of the waveforms in our study appears similar to those described in other reports.[5]

Traditionally, it was assumed that the pulse pressure wave arising from the contraction of the left ventricle in the heart is dampened within the arterial system, so that there is no evidence of the pressure variations remaining at the capillary level.[40] If the pressure waves were damped in this way before reaching the capillary bed, we would not be able to measure rhythmic variations in capillary velocity, as reported here and elsewhere [4,5,19,21,22] In addition, direct measurement of pulse wave propagation through retinal capillaries has recently been confirmed by Bedggood and Metha.[38] An outstanding question is whether the degree of pulsatility observed in flow velocity can be used to infer the compliance of retinal vessels, whereby stiffer vessels are known to be less compliant (and, hence, for example, propagate changes in pressure more rapidly). Measurement of microvascular compliance could provide a powerful tool to measure changes in the stiffness of small vessels that may occur in vascular disease such as stroke. Perhaps relevant to this goal is our observation that pulsatility values were directly related to the systolic rising phase proportions (indicated by quick "abruptness"). It was observed that vessels with steep rising-phase proportions were more pulsatile in nature. This is similar to the findings from nail-fold capillaries where the capillary pulse pressure amplitude (that is, the difference between maximum and minimum pressures) were strongly correlated to the slope during systolic proportion.[41]

Here, we speculate that the reason for observing a range of pulsatility values within a normal individual could be due to the different path lengths taken by blood traveling through different upstream routes to the same vessel bed. In retinal vascular disease, a range of pulsatility values within a capillary bed could indicate that some vessel paths were stiffer, as a result of pathological processes, while other paths remain relatively unaffected. In more advanced disease where all upstream vessels are very stiff (or noncompliant), one could imagine less variability in pulsatility (as well as faster propagation of the pulse wave) throughout the capillary bed. Thus, the pulsatility parameter could be explored in future studies to investigate its potential utility in studying diseased populations.

Variability in Average Velocities. The average erythrocyte velocities reported here are comparable to those of previously published studies using AO imaging. The V_{ave} ± SD (range) values of 1.18 ± 0.46 (0.26–2.30) found here are in close agreement to those reported previously: 1.33 ± 0.28 (1.30–1.80),[7] 1.14 (0.30–2.26),[4] 1.22 (0.58–1.98),[5] and 1.70 (0.93–3.32) mm/s.[6] A mean V_{max} of 1.87 (range, 0.61–3.73) observed here matched very well with previously reported V_{max} values of 1.88 (0.80–3.35)[4] and 1.88 (0.71–3.98).[5] Figure 5 shows that the average velocity is correlated to the maximum. Although this may seem trivial, the very strong degree of correlation may be of use in that the average speed can be reliably predicted if the peak speed is known, both from the point of view of developing fluid mechanical flow models and from the perspective of developing biomarkers that do not require that every vessel has been interrogated for multiple cardiac cycles.

In the current study, using frame rates of 200 to 300 fps, we were able to capture flow information to a maximum velocity of about 3.7 mm/s. We have not reported on vessels with velocities higher than this, as fast-flowing vessels give the appearance of flow reversals and were not suitable for our study. So, our analysis may not be representative of all vessels in a given network. However, it is the best we could do with the available methodology and since we have characterized all vessels with clear single corpuscular flow, the results presented in this study are the best attempt of characterizing flow in a subset of capillary vessels.

Flow Heterogeneity Within a Network

The initial results from our own group were the first, to the best of our knowledge, to indicate that capillary vessels exhibit a greater spatial heterogeneity (relative to the temporal heterogeneity) in a number of flow parameters such as V_{min}, V_{max}, V_{ave}, abruptness, peak time, and period (Neriyanuri S, et al. *IOVS* 2019;60:ARVO E-Abstract 4596). Here, we also explored a number of local vessel factors that can possibly give rise to variability in flow across the vascular network, an investigation that has not previously been undertaken.

Microvascular heterogeneity is not altogether unexpected in metabolically active tissues such as heart, brain, and the retina.[42–44] In the retina, at least two fundamental mechanisms—namely, stochastic angiogenesis and the dimensional problem—have been postulated that might lead to the heterogeneity in microvascular distribution and heterogeneity in local blood flow on a small scale.[45]

Retinal tissue has marked structural and dimensional heterogeneity, with organizations of neurons into distinct cellular nuclear layers separated by synaptic layers. At the level of small vessels (such as capillaries), flow is expected to be very sensitive to even small changes in vessel structure. Flow heterogeneity has thus been postulated to arise as a consequence of heterogeneous intraretinal oxygen consumption to meet the metabolic demands of variably distributed retinal neural cells.[46] Alternatively, Jespersen and Østergaard,[47] modeling capillary transit time heterogeneity in brain, reported that if heterogeneity exists then there is greater spare capacity to shift to more homogeneous states in conditions of physiological stress such as hypoxia and hyperemia, thereby improving overall oxygen extraction efficiency.

Effect of Local Vessel Structural Variables on Flow

For the sample of capillaries included in this analysis, vessel diameters were found to be poorly associated with any of the flow variables in our subjects. This is similar to findings in mouse retina, where vessel diameters did not show any significant associations with the flow velocities in capillary vessels.[22] This is in contrast to the larger vessels, where changes in velocity have been reported following changes in diameter in accordance with Newtonian predictions.[22,48,49] Although we observed that vessel segments with shorter lengths exhibited higher COV (or pulsatility) compared to vessels with longer lengths, no significant relations were found between flow parameters and vessel tortuosity. The significant association between vessel length and

pulsatility is in accord with basic flow mechanics of vessels for any caliber, where the amount of resistance is expected to accrue the greater the length of vessel through which the blood must travel.

The lack of an association between vessel tortuosity and flow parameters is in accord with the predictions of fluid dynamics. Capillaries feature slow flow and narrow diameters, giving them a Reynolds number far less than 1, indicating that the viscous forces far outweigh the contribution of inertial forces acting on the fluid.[26] This means that twists and bends in a vessel that might be expected to result in significant energy dissipation in larger vessels may not have a significant effect at the capillary level.

Local Vessel Flow Variables and Flow Heterogeneity

The local flow variables measured for vessels included LCD and hematocrit. Our findings on average hematocrits (0.41) and their range (0.24–0.57) are similar to those reported in the literature. Mouse retinal capillary hematocrits varied between 0.24 and 0.43.[20] An average hematocrit of 0.49 was noted in mouse retina in another study.[50] These values are comparable to the findings reported in choroid and the brain capillaries in rats.[51] There is a paucity of information on the cell counts in human retinal capillaries, but the findings reported here on LCD and hematocrit should help establish normal ranges in the future.

A proportional relationship between velocity and hematocrit was seen in at least 50% of the vessel segments in our subjects. In general, an increase in velocity with increasing hematocrits indicates adequate oxygen supply to meet the high oxygen demands of the inner retina.[52] Within an individual vessel, as well, a consistent increase in velocity as a function of hematocrit/LCD content was noted, which suggests a plasma redistribution occurring locally with changing velocities. A possible explanation would be that an increased oxygen demand causes the retinal vessels to dilate; in this state, where the vessels have lower resistance, the cells can enter the vessel more readily and therefore the hematocrit can increase.

Study Limitations

The depth of focus of the imaging system may have influenced our diameter measurements, as a focus favoring superficial vessels would appear to blur slightly deeper vessels and vice versa. The depth of focus of our system is approximately 0.05 to 0.10 D (approximately 15–30 µm for an emmetropic eye). Our imaged locations were also close to the edge of the FAZ where there is not much stratification of the retinal capillary beds. Therefore, one would anticipate little error in vessel diameter because of geometric blur. However, the refractive and scattering properties of blood constituents imaged within the capillaries are known to be detectable well outside the vascular lumen, manifesting as secondary bright bands in the motion contrast image. This creates uncertainty in measured lumen diameters, which can be mitigated somewhat by considering the brightest band in the motion contrast image.[25,35,53]

Future Recommendations

As our data were collected adjacent to the foveal avascular zone, we did not consider a sufficiently broad range of retinal locations to analyze any dependency of flow parameters on eccentricity in the retina. We speculate that the avascular zone could be a region of comparatively great oxygen demand because it is the first opportunity for the inner retinal neurons to receive any inner retinal blood supply and because of the high density of neurons in the fovea. Further work is needed to explore this.

Our pilot analysis ($n = 4$ vessels) on temporal heterogeneity (i.e., variations in flow with time) in the same vessel imaged up to five times (spanning 2–38 minutes) showed that the flow parameters varied only minutely. The greatest ranges in V_{max}, V_{min}, abruptness, and pulsatility contrast were recorded as 1.75 to 2.14 mm/s, 0.31 to 0.48 mm/s, 0.19 to 0.33, and 0.38 to 0.52, respectively. These preliminary observations on the stability of flow parameters in the same vessel over time should be confirmed with more observational work.

Conclusions

The results from this study indicate spatial heterogeneity in the characteristics of normal red cell flow through parafoveal capillary networks. The average velocities within a vessel were moderately influenced by the linear cell density and hematocrit content within that vessel. The overall flow among retinal capillaries was not associated with vessel diameter or vessel tortuosity, whereas vessel length was weakly associated with velocity. Because local vessel factors did not significantly influence the flow within a vessel, it would be useful to consider the variables at the network level to further explore which factors drive the observed variations in capillary flow characteristics.

Acknowledgments

Supported by an Australian Government Research Training Program Scholarship (SN) and the Australian Research Council Discovery Project (DP180103393to AM, PAB). Figures 1, 3, 5 and 6 have been reproduced (under CC BY-NC-ND 4.0) from the material presented by the first author (SN) at ARVO 2019, with modifications to Figure 5 (replotted using complete set of data).

Disclosure: **S. Neriyanuri**, None; **P. Bedggood**, None; **R.C.A. Symons**, None; **A.B. Metha**, None

References

1. Wong-Riley MTT. Energy metabolism of the visual system. *Eye Brain*. 2010;2:99–116.
2. Campbell JP, Zhang M, Hwang TS, et al. Detailed vascular anatomy of the human retina by projection-resolved optical coherence tomography angiography. *Sci Rep*. 2017;7:42201.
3. Mutlu F, Leopold IH. The structure of human retinal vascular system. *Arch Ophthalmol*. 1964;71(1):93–101.
4. de Castro A, Huang G, Sawides L, Luo T, Burns SA. Rapid high resolution imaging with a dual-channel scanning technique. *Opt Lett*. 2016;41(8):1881–1884.
5. Gu B, Wang X, Twa MD, Tam J, Girkin CA, Zhang Y. Noninvasive in vivo characterization of erythrocyte motion in human retinal capillaries using high-speed adaptive optics near-confocal imaging. *Biomed Opt Express*. 2018;9(8):3653–3677.
6. Warner RL, Gast TJ, Sapoznik KA, Carmichael-Martins A, Burns SA. Measuring temporal and spatial variability of red blood cell velocity in human retinal vessels. *Invest Ophthalmol Vis Sci*. 2021;62(14):29.

7. Bedggood P, Metha A. Direct visualization and characterization of erythrocyte flow in human retinal capillaries. *Biomed Opt Express*. 2012;3(12):3264–3277.
8. Martin JA, Roorda A. Pulsatility of parafoveal capillary leukocytes. *Exp Eye Res*. 2009;88:356–360.
9. Tam J, Tiruveedhula P, Roorda A. Characterization of single-file flow through human retinal parafoveal capillaries using an adaptive optics scanning laser ophthalmoscope. *Biomed Opt Express*. 2011;2(4):781–793.
10. Tang J, Mohr S, Du YP, Kern TS. Non-uniform distribution of lesions and biochemical abnormalities within the retina of diabetic humans. *Curr Eye Res*. 2003;27(1):7–13.
11. Kern TS, Engerman RL. Vascular lesions in diabetes are distributed non-uniformly within the retina. *Exp Eye Res*. 1995;60(5):545–549.
12. Hudson C, Flanagan JG, Turner GS, Chen HC, Rawji MH, McLeod D. Exaggerated relative nasal-temporal asymmetry of macular capillary blood flow in patients with clinically significant diabetic macular oedema. *Br J Ophthalmol*. 2005;89(2):142.
13. Haj Najeeb B, Simader C, Deak G, et al. The distribution of leakage on fluorescein angiography in diabetic macular edema: a new approach to its etiology. *Invest Ophthalmol Vis Sci*. 2017;58(10):3986–3990.
14. Holm K, Adrian ML. In diabetic eyes, multifocal ERG reflects differences in function between the nasal part and the temporal part of the macula. *Graefes Arch Clin Exp Ophthalmol*. 2012;250(8):1143–1148.
15. Kaizu Y, Nakao S, Yoshida S, et al. Optical coherence tomography angiography reveals spatial bias of macular capillary dropout in diabetic retinopathy. *Invest Ophthalmol Vis Sci*. 2017;58(11):4889–4897.
16. Ikram MK, Cheung CY, Lorenzi M, Klein R, Jones TLZ, Wong TY. Retinal vascular caliber as a biomarker for diabetes microvascular complications. *Diabetes Care*. 2013;36(3):750–759.
17. Burns SA, Elsner AE, Chui TY, et al. In vivo adaptive optics microvascular imaging in diabetic patients without clinically severe diabetic retinopathy. *Biomed Opt Express*. 2014;5(3):961–974.
18. Tam J, Dhamdhere KP, Tiruveedhula P, et al. Disruption of the retinal parafoveal capillary network in type 2 diabetes before the onset of diabetic retinopathy. *Invest Ophthalmol Vis Sci*. 2011;52(12):9257–9266.
19. Bedggood P, Metha A. Adaptive optics imaging of the retinal microvasculature. *Clin Exp Optom*. 2020;103(1):112–122.
20. Guevara-Torres A, Joseph A, Schallek JB. Label free measurement of retinal blood cell flux, velocity, hematocrit and capillary width in the living mouse eye. *Biomed Opt Express*. 2016;7(10):4228–4249.
21. Bedggood P, Metha A. Mapping flow velocity in the human retinal capillary network with pixel intensity cross correlation. *PLoS One*. 2019;14(6):e0218918.
22. Joseph A, Guevara-Torres A, Schallek J. Imaging single-cell blood flow in the smallest to largest vessels in the living retina. *eLife*. 2019;8:e45077.
23. Arichika S, Uji A, Hangai M, Ooto S, Yoshimura N. Noninvasive and direct monitoring of erythrocyte aggregates in human retinal microvasculature using adaptive optics scanning laser ophthalmoscopy. *Invest Ophthalmol Vis Sci*. 2013;54(6):4394–4402.
24. Shigeta A, Akihito U, Sotaro O, Kazuaki M, Nagahisa Y. Adaptive optics-assisted identification of preferential erythrocyte aggregate pathways in the human retinal microvasculature. *PLoS One*. 2014;9(2):e89679.
25. Bedggood P, Ding Y, Metha A. Measuring red blood cell shape in the human retina. *Opt Lett*. 2023;48(7):1554–1557.
26. Fung Y-C. *Biomechanics: Circulation*, 2nd ed. New York: Springer-Verlag; 1996.
27. Balogh P, Bagchi P. Analysis of red blood cell partitioning at bifurcations in simulated microvascular networks. *Phys Fluids*. 2018;30(5):051902.
28. Balogh P, Bagchi P. Direct numerical simulation of cellular-scale blood flow in 3D microvascular networks. *Biophys J*. 2017;113(12):2815–2826.
29. Bagchi P. Mesoscale simulation of blood flow in small vessels. *Biophys J*. 2007;92(6):1858–1877.
30. Duan A, Bedggood PA, Bui BV, Metha AB. Evidence of flicker-induced functional hyperaemia in the smallest vessels of the human retinal blood supply. *PLoS One*. 2016;11(9):1–17.
31. Bedggood P, Metha A. Optical imaging of human cone photoreceptors directly following the capture of light. *PLoS One*. 2013;8(11):1–10.
32. Duan A, Bedggood PA, Metha AB, Bui BV. Reactivity in the human retinal microvasculature measured during acute gas breathing provocations. *Sci Rep*. 2017;7(1):2113.
33. Delori FC, Webb RH, Sliney DH. Maximum permissible exposures for ocular safety (ANSI 2000), with emphasis on ophthalmic devices. *J Opt Soc Am A Opt Image Sci Vis*. 2007;24(5):1250–1265.
34. Tam J, Martin JA, Roorda A. Noninvasive visualization and analysis of parafoveal capillaries in humans. *Invest Ophthalmol Vis Sci*. 2010;51(3):1691–1698.
35. Bedggood P, Metha A. Analysis of contrast and motion signals generated by human blood constituents in capillary flow. *Opt Lett*. 2014;39(3):610–613.
36. Otsu N. A threshold selection method from gray-level histograms. *IEEE Trans Syst Man Cybern Syst*. 1979;9(1):62–66.
37. Bedggood P, Metha A. Recovering the appearance of the capillary blood column from under-sampled flow data. *Opt Lett*. 2020;45(15):4320–4323.
38. Bedggood P, Metha A. Direct measurement of pulse wave propagation in capillaries of the human retina. *Opt Lett*. 2021;46(18):4450–4453.
39. Mukaka MM. Statistics corner: a guide to appropriate use of correlation coefficient in medical research. *Malawi Med J*. 2012;24(3):69–71.
40. Burton AC. *Physiology and Biophysics of the Circulation: An Introductory Text*. Chicago, IL: Year Book Medical Publishers; 1972.
41. Shore AC, Sandeman DD, Tooke JE. Capillary pressure, pulse pressure amplitude, and pressure waveform in healthy volunteers. *Am J Physiol*. 1995;268(1):H147–H154.
42. Hudlicka O, Wright AJ, Ziada AM. Angiogenesis in the heart and skeletal muscle. *Can J Cardiol*. 1986;2(2):120–123.
43. Patel-Hett S, D'Amore PA. Signal transduction in vasculogenesis and developmental angiogenesis. *Int J Dev Biol*. 2011;55(4-5):353–363.
44. Pries AR, Secomb TW, Gaehtgens P. Structure and hemodynamics of microvascular networks: heterogeneity and correlations. *Am J Physiol*. 1995;269(5):H1713–H1722.
45. Pries AR, Secomb TW. Origins of heterogeneity in tissue perfusion and metabolism. *Cardiovasc Res*. 2009;81(2):328–335.
46. Yu D-Y, Cringle SJ, Paula KY, et al. Retinal capillary perfusion: spatial and temporal heterogeneity. *Prog Retin Eye Res*. 2019;70:23–54.
47. Jespersen SN, Østergaard L. The roles of cerebral blood flow, capillary transit time heterogeneity, and oxygen tension in brain oxygenation and metabolism. *J Cereb Blood Flow Metab*. 2012;32(2):264–277.
48. Zhong Z, Song H, Chui TYP, Petrig BL, Burns SA. Noninvasive measurements and analysis of blood velocity

Investigative Ophthalmology & Visual Science

profiles in human retinal vessels. *Invest Ophthalmol Vis Sci*. 2011;52(7):4151–4157.

49. Palochak CMA, Lee HE, Song J, Geng A, Linsenmeier RA, Burns SA, et al. Retinal blood velocity and flow in early diabetes and diabetic retinopathy using adaptive optics scanning laser ophthalmoscopy. *J Clin Med*. 2019;8(8):1165.
50. Paques M, Tadayoni R, Sercombe R, et al. Structural and hemodynamic analysis of the mouse retinal microcirculation. *Invest Ophthalmol Vis Sci*. 2003;44(11):4960–4967.
51. Seylaz J, Charbonné R, Nanri K, et al. Dynamic in vivo measurement of erythrocyte velocity and flow in capillaries and of microvessel diameter in the rat brain by confocal laser microscopy. *J Cereb Blood Flow Metab*. 1999;19(8):863–870.
52. Cringle SJ, Yu DY, Yu PK, Su EN. Intraretinal oxygen consumption in the rat in vivo. *Invest Ophthalmol Vis Sci*. 2002;43(6):1922–1927.
53. Guevara-Torres A, Williams DR, Schallek JB. Origin of cell contrast in offset aperture adaptive optics ophthalmoscopy. *Opt Lett*. 2020;45(4):840–843.

Investigative Ophthalmology & Visual Science